Available online at www.sciencedirect.com

ScienceDirect

Journal of the European Ceramic Society 34 (2014) 3791–3800

www.elsevier.com/locate/jeurceramsoc

Model for Vickers microhardness prediction applied to SnO_2 and TiO_2 in the normal and high pressure phases

Maria A. Caravaca [a,*], Luis E. Kosteski [c], Julio C. Miño [a], Ricardo Barrios D'Ambra [a], Bruno Uberti [a], Ricardo A. Casali [b]

[a] *Facultad de Ingeniería, Universidad Nacional del Nordeste, Resistencia, Argentina*
[b] *Facultad de Ciencias Exactas, Naturales y Agrimensura, Universidad Nacional del Nordeste Corrientes, Argentina*
[c] *Mechanical Engineering, Universidade Federal do Pampa Rio Grande do Sul, Brazil*

Received 28 December 2013; received in revised form 17 April 2014; accepted 19 June 2014
Available online 16 July 2014

Abstract

The Vickers microhardness of TiO_2 is calculated using elastic properties obtained by first principles calculations combined with Discrete Elements Method (DEM). The calculation is carried out in rutile and cotunnite phases. It was found that rutile phase, has a microhardness of 8.6 GPa and 12.8 GPa for the failure and fracture modes in agreement with experimental results range. In cotunnite phase the hardness for failure and fracture mode are 24.1 and 24.4 GPa, close to 26 GPa, applying Simunek model. To give insight to this methodology, the calculation is extended to SnO_2 in the normal phase. The microhardness value obtained in the failure mode is 2.67 GPa. The method developed here, to obtain the Vickers microhardness, could be applied to a systematic study of tailoring materials. Since hardness is related to elastic shear properties, our results can be used as an assessment of the material properties as solid lubricating at first order.
© 2014 Elsevier Ltd. All rights reserved.

Keywords: Elastic constants; Microhardness; Toughness ceramics

1. Introduction

TiO_2 represents a typical anisotropic elastic material. Some manufacturing processes require micromechanical modeling of materials in terms of single crystal for custom tailoring new composite materials. Moreover, the study of the relative stability of the phases and their elastic properties are well motivated by, for example, the understanding about the chemical bonds and the cohesion of the material. Hardness, defined as the material resistance to localized deformation, is an important mechanic property of materials. Hard materials have many industrial applications wherever resistance to abrasion and wear are important. The experimental data for a wide variety of materials shows that the shear modulus, which measures the material's resistance to shape change, is correlated to hardness. In order to deduce a computational scheme for simulating hard materials, the shear modulus associated with the various slip systems encountered in crystalline structures are expressed, for the first time, by means of the microscopic parameters of the chemical bonds, in the framework of the density functional theory.[1–3] Accurate experimental determinations of elastic constants require the use of large pure single crystals which, in the case of many ceramics, are difficult to obtain. Thus *ab initio* theoretical studies which provide elastic properties of single and poly-crystals could be substantial contributions.

The discovery of cotunnite, orthorhombic OII phase, stabilized at 60 GPa, that was able to be held at 77 K and normal pressure with a clean, flat surface on which indentation hardness measurements were performed is constructed as evidence of a material that could be classified as superhard, although this is not devoid of controversy.

Dubrovinsky et al.[4] made measurements to determine the microhardness Vickers using nine indentations. They reported values in the range 36.8–40.7 GPa, results independent of the load.

* Corresponding author. Fax: +54 3624428106.
E-mail addresses: mac@ing.unne.edu.ar, mariacaravaca_ar@hotmail.com (M.A. Caravaca).

http://dx.doi.org/10.1016/j.jeurceramsoc.2014.06.022
0955-2219/© 2014 Elsevier Ltd. All rights reserved.

Recent studies have shown that hardness, a complex property, can be calculated using very simple approaches or even analytical formulas. These model approaches can help to reappraise controversial experimental results as shown by Oganov and Lyakhov.[5,6]

Based on the idea that the hardness of covalent crystal is intrinsic and equivalent to the sum of the resistance to the indenter of each bond per unit area, a semi-empirical method for the evaluation of hardness of multicomponent crystals was presented by Gao et al.[7] They found that bond density or electronic density, bond length, and degree of covalent bonding are three determinative factors for the hardness of a polar covalent crystal. This method initializes a link between macroscopic property and electronic structure from first principles calculation.

By other hand, the widely applied Teter's[8] empirical correlation between hardness and shear modulus has been considered to be not always valid for a large variety of materials. The main reason is that shear modulus only responses to elastic deformation whereas the hardness links both elastic and permanent plastic properties.

Chen et al.[9] found an intrinsic correlation between hardness and elasticity of materials that correctly predicts Vickers hardness for a wide variety of crystalline materials as well as bulk metallic glasses (BMGs) if the material is intrinsically brittle. Their results demostrate that the hardness of polycrystalline materials can be correlated with the product of the squared Pugh's modulus ratio $k = G/B$ and the shear modulus. It is capable to correctly predict the hardness of all hard compounds known.

The theoretical hardness of crystals can be estimated from the semi-empirical theory. For instance, by mean of the method proposed by Simunek[10] and coworkers.

Zhou et al.[11] gave an interesting model based on the fact that both hardness and vibrational Raman spectrum depend on the intrinsic property of chemical bonds. They propose a new theoretical model to predict hardness of a covalent crystal. The quantitative relationship between hardness and vibrational Raman frequencies deduced from the typical zinc-blenda covalent crystals is validated to be also applicable for the complex multi component crystals. This model enables to characterize, non-destructively and indirectly, the hardness of novel super hard materials synthesized under ultra-high pressure condition with the *in situ* Raman spectrum measurement.

The prediction of hardness in the normal phases, which are well established for the elastic properties of rutile phase, helps to discern the predictive power of calculation in this type of oxides. Then it can be applied to cases where direct measurement of the elastic properties is not accessible and in those where a systematic search of new solid lubricants is required.

High pressure studies of materials are often tricky, and the field of high-pressure research is full of both exciting discoveries and miss discoveries. For instance, it has been claimed[4] that TiO_2–cotunnite, quenched from high pressure, where the samples, as a consequence of performing the experiment in an electrically-heated DAC are cylindrical in shape, is the hardest known oxide with a Vickers hardness of 38 GPa, but this claim has been hotly debated.

It is difficult to experimentally appraise such results obtained on tiny samples given that indentation size effect is one of the several size effects on strength for which "smaller is stronger", as found by Pharr[12] that the size effect is manifested as an increase in hardness with decreasing depth of penetration and becomes important at depth of less than approximately 1 μm. Furthermore at lower level of the load in microhardness indentation test results in a higher apparent micro-hardness. This is known as the indentation load/size effects (ISE) and this load dependence of hardness has been traditionally described through the application of Meyer law.[13]

This indentation load/size effects on the microhardness has been considered on the basis of a variety of phenomena: work hardening during the indentation; the load to initiate plastic deformation; the activation energy for dislocation nucleation and more. The cause of this effect for two rutile structure single crystal, TiO_2 and SnO_2 has been achieved, applying Hays and Kendall approach[14] in the examination of Knoop indentation measurements.[15] They have shown that ISE is a consequence of the indentation-size which is proportional to the resistance of the test specimen to the plastic deformation. This implies the existence of a minimum level of the indentation test load, below which plastic deformation does not initiate, but only elastic deformation occurs. Then the experimental indentation size measurements are not directly related to the load applied but rather to effective indentation test load (P–W) where W is the material resistance to the initiation of plastic flow.

The theoretical models could help to distinguish facts from artefacts in the experimental results. In the models presented by Organov,[5] the hardness of TiO_2 cotunnite varies in the range 7–20 GPa. Based on the extended model,[7] was found to be 15.9 GPa, softer than common corundum, Al_2O_3 (21 GPa), stishovite SiO_2 (33 GPa),[16] or B_6O (45 GPa).[17] The low hardness of TiO_2–cotunnite is due to the non-depicted bond iconicity and high coordination number of Ti (nine-fold), *i.e.* relatively weak and non-directional Ti–O bonds. Moreover, the pronounced anisotropy and the fact that shear elastic constants are relatively weak compared to the axial ones,[18] could suggest that ultra hard TiO_2–cotunnite is the result of enhancements of the surface resistance to the initiation of plastic deformation due to the pressurized processes, and not natural resistance to the localized deformations. This could be discerned if a measurement of dynamic hardness is done and shown the portion that corresponds to both plastic and elastic indentation work.

While the connection between the hardness and elastic properties is beyond doubt, it is complex to solve the analytical problem of penetration of an indenter. The current status of various theoretical approaches given the "prediction" of material hardness has been reviewed by Tse.[19] It is shown that the simple empirical correlation with the shear modulus generally provide good estimates of the Vickers hardness. Semi-empirical models based solely on the strength of chemical bonds, although performed as well, are theoretically incomplete. First-principles calculations of the elastic constant and derived properties like shear strength is perhaps the most reliable theoretical approach to compare with experiment results.

In this work, microscopic first-principles calculations and numerical methods, based on fracture mechanics, are combined to give a new hardness values for TiO_2 in the controversial cotunnite phases. Given that rutile TiO_2 is a technologically important material in heterogeneous catalysis, as a pigment and as an opacifier, our calculation includes elastic properties and hardness in the normal phase rutile.

On the other hand, tin dioxide (SnO_2) is an industrially important material which is used in numerous applications where the specific electrical, optical and mechanical properties of SnO_2 are highly desirable.

For example, SnO_2 is used extensively as the active material in gas sensors,[20–23] as well as in systems where optical or electrical coatings are required, such as in low-emissivity architectural glass solar cells,[24] and liquid crystal displays.[25]

Moreover, SnO_2 undergoes a structural transition to Pnmn phase at 12 GPa but the transition pressure is reduced to lower value by one order of magnitude, when a residual non-hydrostatic pressure is present.[26] This material has a phase diagram whose order under pressure is consistent with the diagram of SiO_2 (at very high pressures).[27] Consequently SnO_2 is a prototype for the study of transformations and elastic anisotropies of the SiO_2 at laboratory scale, the largest component of the earth's crust, given that there is a complete analogy to the sequence of the phase transformations experienced by the tin oxide. Thus an indirect study of the SiO_2 is possible and very useful, because the high pressures involved in the silica phase-transitions would not be achievable at laboratory scale.

We apply first-principles method to obtain the elastic constants in single crystal of TiO_2 and SnO_2 and derivatives properties in the polycrystalline approach. To determine the microhardness Vickers (H_V), we use a numerical truss-like Discrete Element Method (DEM). This requires a parameter representing a maximum tensile strength, among others. In this work, it is obtained from the strain-stress relationship for the weakness C_{44} elastic constants calculation. The indentation procedure applied in DEM is similar to that used to obtain the hardness in Al_2O_3.[28]

2. Methods

2.1. First-principle method

The study of the structure and elastic properties of TiO_2 and SnO_2 was carried out with the SIESTA *ab initio* method.[29] This code is shown to give a good description of the structural and elastic properties of Hf oxides and their polymorphisms,[30] as well as TiO_2 in rutile and cotunnite phases[18] and recently SnO_2.[31]

SIESTA code has been developed and implemented in a self-consistent Density Functional Theory (DFT) scheme using standard norm-conserving pseudo-potentials and a flexible, numeric linear combination of atomic orbital basis set, which includes multiple-zeta and polarization orbitals.

Exchange and correlation are treated with the local density approximations. The basis functions and the electron density are projected on a real-space grid in order to calculate the Hartree and exchange-correlation potentials. Forces and stresses are also calculated efficiently and accurately, thus allowing structural relaxation and molecular dynamics simulations.

The Bravais lattice in rutile (Fig. 1a) and cotunnite phases (Fig. 1b) are defined by the vectors: (a, a, c) and (a, b, c) respectively. The equilibrium lattice and elastic properties of TiO_2 used here were studied in detail in converged calculations.[18] Applying to the equilibrium lattice small deformations through the matrix D according to the symmetry of the crystal, the stress tensor for TiO_2 and SnO_2 in rutile phases was obtained. Fitting the results to Hooke's law, the elastic constants are obtained and the directional Young's modulus can be constructed. The maximum strength is approximated to the higher value of shear stress obtained from the stress–strain relationship related to the C_{44} (C_{55}). This is due to the Vickers hardness imprint is measured on the crystallographic plane (1 1 0)[32,33] and the tip of indenter exerts the stress in (0 1 1) and (1 0 1) crystalline plane. Respect to the polycrystalline description of the mean values of elastic properties, the Voigt–Reuss–Hill (VRH) approach is applied to the oxides studied here.

2.2. Truss-like Discrete Element Method

The Discrete Element Method (DEM) was originally developed by Cundall et al.[34] to solve rock mechanics. Today, it is widely accepted as an effective method of addressing engineering problems in granular and discontinuous materials. The version of the truss-like Discrete Element Method (DEM) proposed by Riera[35] in 1984 employed in this paper consists of treating a continuous medium as regular repetition of discrete basic units[36] (Fig. 2).

The rigidity of the represented truss bars are equivalent to the continuum that is being represented. Since they are considered as spatial truss bars, each node accounts for three degrees of freedom. The mass of the model is made discrete and concentrated on the nodes of the mentioned unit in a way to reproduce the trial density of mass of the system.

A uniaxial relation between the axial forces *vs.* strain for the bars following the bilinear softening law, proposed by Hillerborg,[37] was adopted for the representation of material. This law, shown in Fig. 3, allows accounting for the irreversible effects of crack nucleation and propagation. In Fig. 3, P_{cr} represents the maximum tensile force transmitted by the bar, and ε_p is the deformation (strain) associated with P_{cr}.

E_A is the cubic model bar rigidity, equal to the product of the material Young Modulus, E, by the cross sectional area of the element A.[35] This verify that $P_{cr} = \varepsilon_p$. E_A, k_r is the ductility, by which the strain at the bar no longer transmit tensile force, ε_r.

The deformation limit ε_r is chosen to meet the condition that when an element fails and cracks opens, certain amount of energy (G_f) is released. The general relationship between ε_p and G_f was established as a condition for traction failure and its deduction is based on the Mechanics of Linear Elastic Fracture Eqs. (1) and (2).

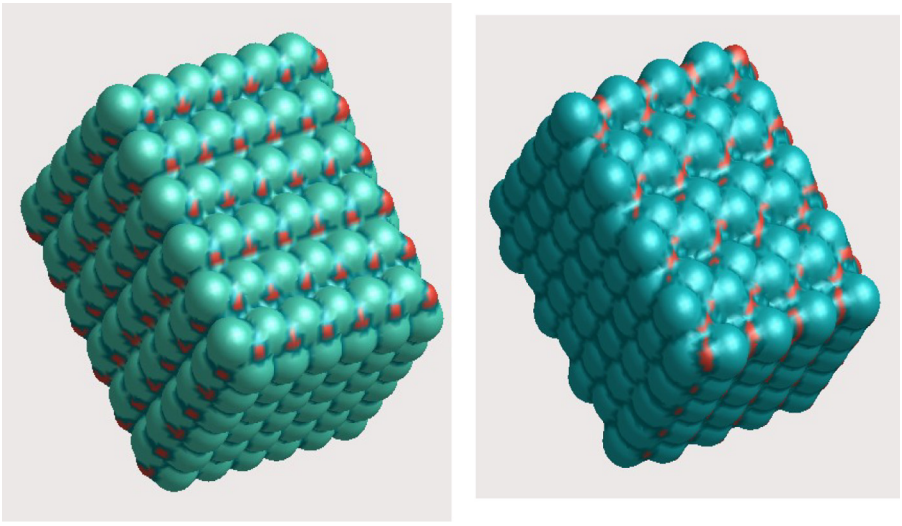

Fig. 1. TiO_2 in (a) rutile and (b) Pnma phases (plane 1 1 0).

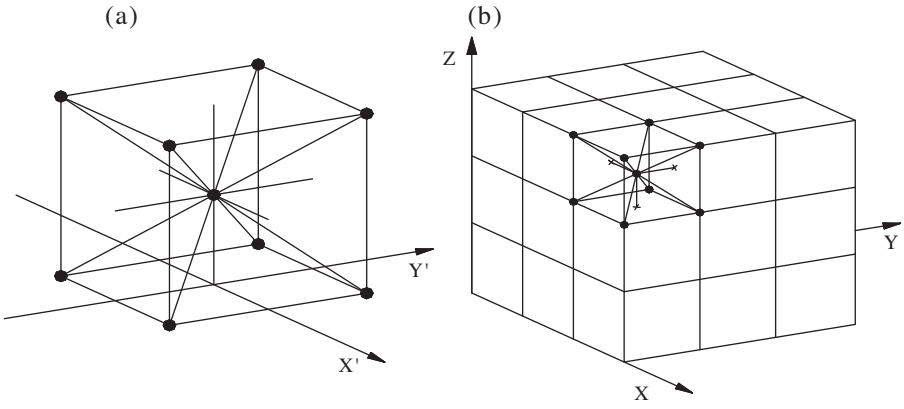

Fig. 2. (a) DEM basic cubic module, (b) modules composing the prism.

This fracture energy is

$$G_f = K_f^2 \left(\frac{1 - \nu^2}{E} \right) \tag{1}$$

This equation tells us that under smaller plasticity condition the propagation of the crack is controlled by G or K_f. It is necessary to maintain the plane strain condition with little plasticity that the crack does not exceed the size of the plastic zone on the edge of the crack (more details in Supplementary page).

$$K_f = \sigma \cdot \pi^{1/2} \cdot a^{1/2} \tag{2}$$

The bar stress is

$$\sigma = \chi \cdot P_{\in r} = \chi \cdot \varepsilon_p \cdot E_A \tag{3}$$

where χ is a geometry-dependent parameter.

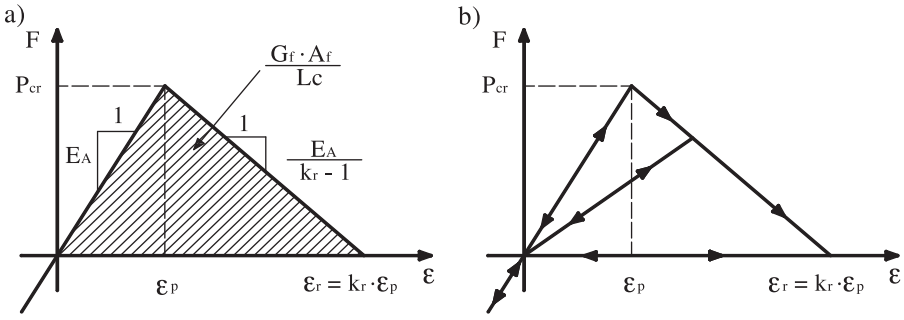

Fig. 3. Relationship of the bars in the elemental cubic arrangements. (a) Constitutive diagram with control parameters; (b) load and unload scheme.[31]

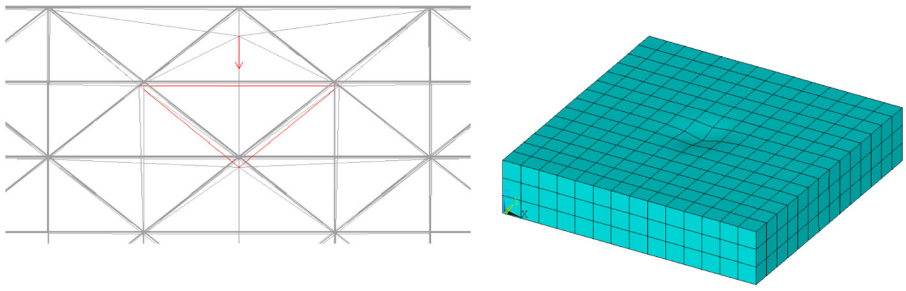

Fig. 4. Load process at 2.0×10^{-9} seg.

Applying (2) and (3) in Eq. (1)

$$\varepsilon_p = R_f \cdot \left[\frac{G_f}{(1-\nu^2) \cdot E_A} \right]^{1/2} \quad (4)$$

where $R_f = \frac{1}{\chi \cdot a^{1/2}}$ is the failure factor.

In Fig. 3 A_f is the effective area where the bar action is distributed.[38] As was defined early, the ductility in DEM is represented by k_r and it can approximate to the ratio between L_{cr} to the length at which the failure occurs. L_c is the basic cubic module length (Fig. 2a).

$$k_r = \frac{L_{cr}}{L_c}$$

The ideal condition of fragile system is k_r value equal or greater than 1. It is important to note that the bar has a linear elastic behavior, with a breakdown of the global model, when compressed by indirect tensile (Poisson effect). A restriction to the Poisson Modulus value to $\nu = 0.25$ must be imposed to achieve an agreement between the cubic arrangement and the represented elastic solid. For other values of ν, certain discrepancies appear in terms of shear, but become negligible when interest is put upon the non-linear result of the studied system.

Since the values of G_f, ε_p and E_A are input data that we have, the value of k_r is affected by L_{cr}. The step increment time (Δt) in the dynamic simulation must be less than the critical one. In our case the critical value of 1.45×10^{-11} seg, is obtained in terms of the mass density, elasticity modulus and indicates the time when an elastic waves passes through a bar element. R_f can be also calculated as a function of k_r and L_c. When values for the other variables are defined, the value of L_c is fixed. Detailed description is found in Refs. 38, 39. The toughness value, necessary for this modelling cannot be obtained by our calculations. Literature values would be employed.[40]

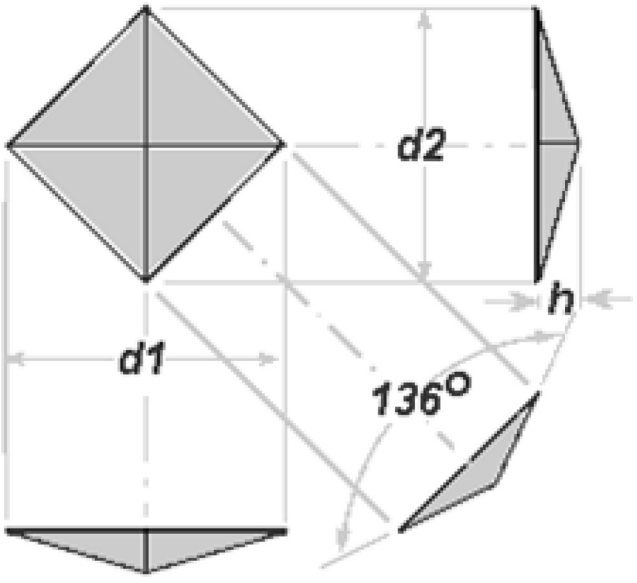

Fig. 5. Permanent impression by the indentator.

2.2.1. Measuring hardness with DEM.

It is essential to model the "strain-softening" effect for a correct representation of the phenomenon of rupture in a brittle material. The softening ("strain-softening") present in the adopted diagram (Fig. 3) aims to put a condition on the amount of energy to be consumed in breaking the material.

For numerical simulation of the hardness in the tetragonal phase (P42/nmc) and orthorhombic ones (Pnma), the values of the parameters used by the DEM, are derivatives of the elastic constants obtained from *ab initio* calculations. The simulated material is originally orthotropic, but DEM approximation imposes, to the determination of the hardness, that an isotropic material to be rendered. In an isotropic material, constant C_{ij} depends on Young's modulus (E) and Poisson's ratio. For provide to DEM a representative E, we calculated first the averaged uniaxial elastic constants of C_{11} C_{22} C_{33} obtained from *ab initio* calculations. This mean value is considered "C_{11}" in

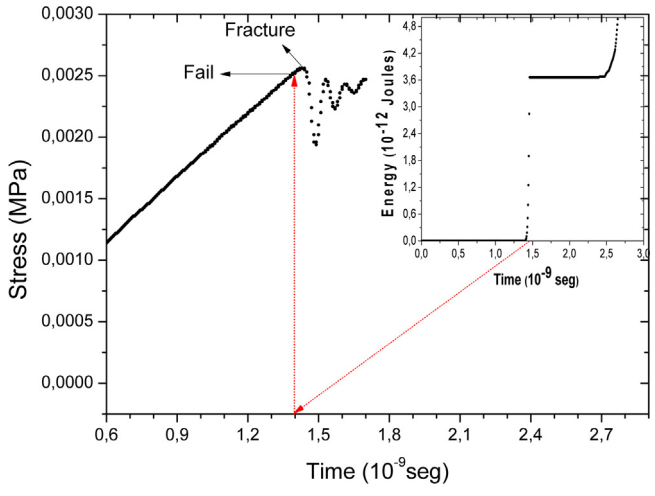

Fig. 6. Damage energy curve (inset) at the time in which the fail occurs in the stress–time function.

Table 1
Calculated elastic constant values of rutile TiO_2 compared to availble experimental data. All units of C_{ij} are in GPa.

Elastic Constant	TiO_2							
	Rutile				Pnma			
	Siesta	Th.[41]	Exp.[45]	Exp.[46]	Exp.[47]	Siesta	Th.[42]	Th.[43]
C_{11}	340	366	268	273	266	688	555	563
C_{22}						510	408	645
C_{33}	470	606	484	484	470	649	450	782
C_{12}	143	225	175	178	173	258	234	330
C_{13}	154	224	147	149	136	240	237	254
C_{23}						253	196	343
C_{44}	181	189	124	125	128	129	89	231
C_{55}						133	109	203
C_{66}	204	272	190	194	188	204	159	254

Table 2
Calculated elastic constant values of rutile SnO_2 compared to available experimental data. All units of C_{ij} are in GPa.

Elastic Constant	SnO_2			
	Rutile			
	Siesta[31]	Th.[47]	Exp.[44]	Th.[48]
C_{11}	261	267	262	261
C_{33}	483	471	450	472
C_{12}	211	179	177	180
C_{13}	161	150	155	150
C_{44}	107	108	103	109
C_{66}	232	222	207	223

DEM constitutive matrix[52] and E is then adjusted to be E_A. The values of the Constitutive Elementary Relation (CER) ε_p (ε_{44}) and E_A (E) would be fitted as well as possible to the maximum strength value σ_{44} obtained through *ab initio* calculations. The toughness value, necessary for this modeling cannot be obtained by our calculations. Literature values would be employed.[40]

In DEM modelling, the critical length of the bars and the Poisson ratio are 2.00×10^{-7} m and 0.25 respectively. The parameter δ[52] which linearize the elastic constants for the model of bar employed by DEM, is 1.125. This value is kept constant in all calculations.

In order to make DEM convergence better, values greater than 1 are applied to ductility k_r. The method can describe the hardness in different modes: the failure and fracture mode. The failure mode refers to the moment, in the simulation, in which the bar "fails", interpreted in the sense that the damage energy (Fig. 6) becomes different to zero.

The fracture of the material corresponds to the instant in which the global model stress–time curve has a constant path and the first break on damage energy curve appears (Fig. 6). At this point, the deformation value is $\varepsilon = \varepsilon_r$, at which the bar no longer transmits energy.

The indentation process consists of two steps: loading (applying maximum load for a few seconds) and unloading (see Fig. 4).

After this process, the permanent impression left by the indenture is measured (Fig. 5) and H_V is calculated using Eq. (5).

$$H_V = \frac{2 \cdot F \cdot sen\frac{136^\circ}{2}}{d^2} \approx 1854 \cdot \frac{F}{d^2} \qquad d = \frac{d1 + d2}{2} \tag{5}$$

Table 3
Calculated thermo-elastic and acoustic properties of polycrystalline TiO_2 using VRH approach, compared with available theoretical and experimental data. E_0, ν, V_t, V_l, V_m, ρ, and θ_D are the Young modulus, Poisson constant, transverse, longitudinal and averaged speed of sound, mass density and Debye temperature, respectively.

Polycrystalline properties	TiO_2					
	Rutile			Pnma		
	Siesta	Exp.[49]	Exp.[46]	Siesta	Th.[42]	Exp
Bo (GPa)	225	228	216	370	301	312(34)[60] 306(9)[61] 431(10)[4]
Go (GPa)	154	115	127	162	119	
E_0 (GPa)	376	285[a]	318	425	314[a]	
ν	0.22	0.28[a]	0.25	0.31	0.33[a]	
V_t (m/seg)	5999	5119[a]	4261	5436	4647[a]	
V_l	10,031	9214[a]	7421	10,327	9145[a]	
V_m (th.)	6639	5702[a]	4733	6078	5208[a]	
ρ (kg/m^3)	4280	4260[a]	6990	5490	5490	
θ_D (k)	933	893	615	775[a]	775[a]	

[a] Calculated here with VRH approach.

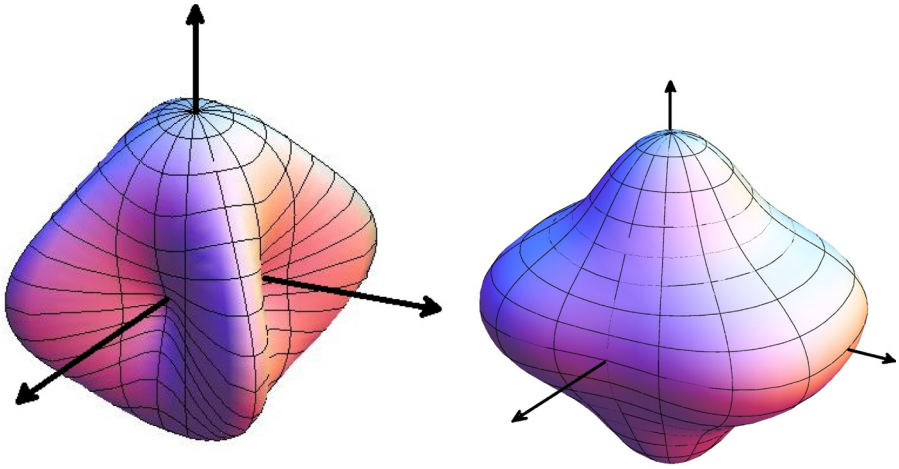

Fig. 7. Young modulus anisotropy for (a) rutile (left), (b) cotunnite (right) structures.

Table 4
Calculated thermo-elastic and acoustic properties of polycrystalline SnO_2 using VRH approach, compared with available theoretical and experimental data. E_0, ν, V_t, V_l, V_m, ρ, and θ_D are the Young modulus, Poisson constant, transverse, longitudinal and averaged speed of sound, mass density and Debye temperature, respectively.

Polycrystalline properties	SnO_2		
	Siesta[31]	Exp.[47]	Th.[48]
Bo (GPa)	225	212[a]	213
Go (GPa)	96	115[a]	106
E_0 (GPa)	253	294[a]	–
ν	0.31	0.27[a]	–
V_t (m/seg)	3707	4072[a]	3840
V_l	7167	7243[a]	7002
V_m (th.)	4150	4531[a]	–
ρ (kg/m^3)		6990	–
θ_D (k)	542	742[a]	565

[a] Calculated here with VRH approach.

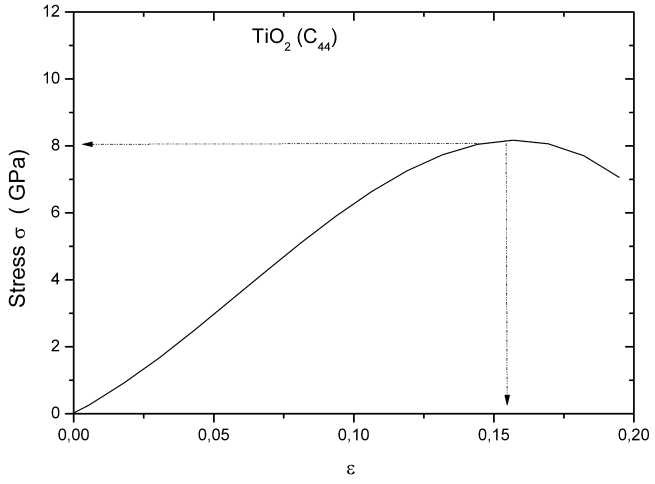

Fig. 8. Stress-strain relationship. For the calculation of C_{44} linear regime is used. The maximum value is considered as a $\boldsymbol{\sigma_F}$ by DEM.

3. Results

3.1. Elastic properties of single crystal and polycrystal

Tables 1 and 2 show the calculated elastic constants for rutile and cotunnite phases of TiO_2 and rutile SnO_2 respectively where available theoretical[41–43,47] and experimental[44–46] data are included for comparison. Tables 3 and 4 show thermo-acoustic properties in the polycrystalline approximation using VRH approach, with data taken from Tables 1 and 2. These B, G values are introduced in the Chen model[9] to obtain, the compound hardness to be compared with DEM results.

In Fig. 7a and b, anisotropic Young modulus in single crystals is shown, obtained from the elastic constants in cotunnite and rutile phase at normal pressure.

As was mentioned, the maximum strength value for parameterizing DEM is chosen to be the higher shear stress σ_{44}. An example is shown for the cotunnite phase in Fig. 8.

3.1.1. Microhardness Vickers

3.1.1.1. TiO_2 in the rutile phase. TiO_2 in the rutile phase (Fig. 1a), has a density of 4280 kg/m^3. To parameterize DEM method, the maximum strength σ_{max}, as was mentioned, is obtained from the stress–strain relationship for the weakest of the calculated elastic constants C_{44}. The highest σ_{44} value found in rutile is 2.7 GPa. To include the fracture propagation velocity in DEM, the 60% of the mean sound velocity obtained from the VRH approach, was considered.

In order to build the isotropic constitutive matrix used in DEM, its first three upper diagonal elements were replaced with the average of the crystal axial values C_{11}, C_{22} and C_{33} (Table 1). This mean value is equal to 380 GPa and named as "C_{11}" in equations quoted in Ref. 52. Given C_{11} we obtained the E_A value and from the second equation of Ref., 52 C_{12} (C_{44}). It should be noted that E_A now turn out to be slightly higher (0.09%) than that E obtained with the VRH approximation (376 GPa).[31] The microhardness Vickers H_V in failure mode is 8.64 GPa and in the fracture mode is 12.28 GPa. Hardness H_V in the failure mode has a small variation with respect to toughness for the range between 1.60 and 2.0 MPa m$^{0.5}$ (Fig. 9). In this phase our results are in agreement with the experimental range values 8.2–12.8 GPa (Table 5) of H_V.

Applying other theoretical models for the calculation of H_V, for instance the Chen et al. model[9] and using experimental data for G and B[44] results H_V between 11.4 and 15.3 GPa. With the

Table 5
Calculated hardness values for TiO_2 and SnO_2 and their comparison with different published models. Here G_f, k_r, σ_F, H_V means fracture energy, the ductility in DEM, the maximum strength and Vickers hardness, respectively. See also our previous calculations in Ref. 51.

Phases		Toughness (MPa m$^{0.5}$)	G_f (N/m)	k_r	σ_F (GPa)	H_V (Gpa)					
						DEM		Exp.	Model		
						Failure	Fracture		Gao	Chen	Zhou
TiO_2	Rutile	1.6	11.31	1.5	2.70	8.64	12.28	8.2–12.8[50] 11.9[32]	9.1[a]	11.4[48] 11[a] 12[a] 5.7[57,b] 15[41]	8.3[62]
	Cotunnite	4.0	3.98	1.1	8.0	24.08	24.21	38[4]	20[a]		–
SnO_2	Rutile	1.8	15.28	22.7	0.78	2.67	–	3.68[31]	8.19[a]	12.7[31] 7.7[a]	16[63]

[a] Calculated using results from SIESTA-LDA.
[b] Calculated with GGA.

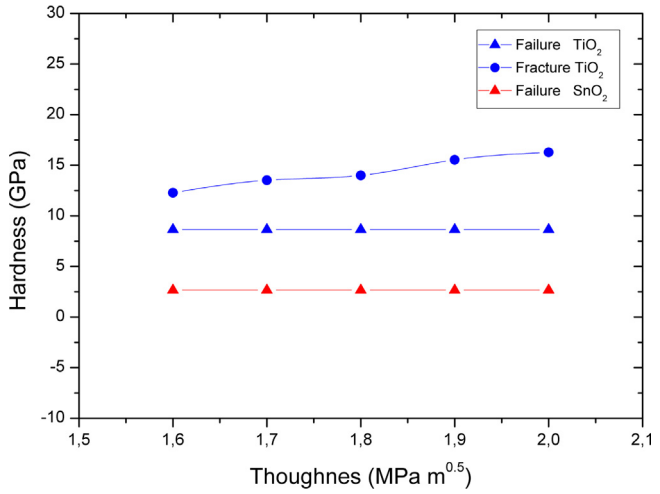

Fig. 9. Hardness–toughness relationship for rutile structure in DEM calculation.

Gao model,[6] $H_V = 9.1$ GPa. Using the proposal by Zhou et al.,[11] where was included from the Raman spectra by Nicol et al.[62] the frequencies and the intensities relative to 720 cm^{-1}, the hardness is 8.3 GPa. All this results, shown in Table 5, are in general agreement with our model, and with the experimental mentioned range.

3.1.2. High pressure phase orthorhombic TiO_2

TiO_2 in the cotunnite phase (Fig. 1b), has a density of 5494 kg/m^3. The maximum strength σ_{max}, in this phase is obtained again from the stress–strain relationship, σ_{44}–ε_{44} (see Fig. 8). The highest σ_{44} (σ_{max}) value found is 8 GPa. As it mentioned earlier, "C_{11}" value of 616 GPa is obtained from the average of our calculated axial elastic constants. The relationships[52] provide the E_A value 513 GPa, 15% higher than the value given by VRH polycrystalline approach ($E = 425$ GPa). The remaining C_{12} (C_{44}) was determined using a Poisson's coefficient of 0.25.[52] The toughness for this high density phase is unknown. It is here approached, in a range of values between 2.77 MPa m$^{0.5}$ (Al_2O_3)[40] and 6.6 MPa m$^{0.5}$, found in ZrO_2 stabilized with CeO_2. In the TiO_2 orthorhombic phase the H_V value is 24.08 GPa in failure mode and does not depend on toughness. In the fracture mode, hardness has very small variation with respect to toughness: for values between 4.0 and 5.5 MPa m$^{0.5}$, the hardness H_V was found to lie between 24.21 and 24.41 GPa.

The difference found between the theoretical predictions and experimental results could be explained based on the indentation load/size effect (ISE). This effect is found in microhardness measurements in single crystal at precisely two structures of rutile TiO_2, SnO_2.[15] ISE is explained on the basis of the work hardening during indentation[53,54] and the activation energy for nucleation of dislocations.[55] But according to Kendall–Hays approximation of ISE, there is a minimum level of indentation load (W) below which plastic deformation does not initiate, but only elastic deformation occurs. In a study by Li and Bradt[15] on a number of hardness measurements in single crystals of SnO_2 and TiO_2 was found that these minimum levels depend on the surface crystallographic orientation. Taking the average of their published results (Table 2 of Ref. 15), we obtain in the case of

rutile-TiO_2, a load (W) equal of 22 g. If the hardness measurements of Dubrovinsky et al., using loads in the range 25–300 g in samples of cotunnite-type TiO_2 recovered cryogenically at 77 K, are corrected with this minimum load, the resulting H_v is found[56] to be about 31 GPa, in fair agreement with our predictions based on the elastic properties of cotunnite TiO_2. To compare with other theoretical models, we also estimated the hardness using the model of Chen[9] where the B and G moduli are calculated applying VRH approach to the elastic constants obtained with SIESTA. The H_V is 11.9 GPa. A recent calculation using CASTEP method[57] together with the Simunek et al. model,[10] gives $H_V = 26.05$ GPa in good agreement with our prediction. Applying the Gao model, we found a value of 20 GPa. If our σ_{44} is replaced in the Lazar et al.[58] prescription, in which the hardness of an intrinsically brittle material, is related to the minimum critical stress for brittle cleavage $\sigma_{C\,\min}$, the hardness results in 8 GPa. Unfortunately it is not possible to compare with Zhou model since there is not available measurement of Raman spectrum in cotunnite TiO_2. It could be desirable to dispose of a Raman spectrum in this high pressure phase.

3.1.3. SnO_2 in the semiconductor rutile phase

Tin oxide represents a semiconductor with a wide band gap and with a covalent character of the bond. In this tetragonal phase (Fig. 8), the density is 6990 kg/m^3. The calculated elastic constants from *ab intio* method are used to obtain the average matrix elements as was done in TiO_2, setting "C_{11}" to 306 GPa (Table 1– SnO_2). Applying the equation[52] a value $E_A = 255$ GPa is found. The remaining matrix elements for C_{12} (C_{44}) are determined, as was mentioned. The microhardness Vickers was calculated to be 2.67 GPa, only in failure mode because the fracture mode does not satisfy the DEM condition shown in Fig. 6. This is 27% less than the more recently experimental value of 387 H_V (3.68 GPa) found by Ouni et al. 32 The hardness calculated with Chen model using the B and G moduli obtained with SIESTA, is 7.7 GPa, but if the experimental values are used instead,[45] the hardness is 12.7 GPa (see Table 5). If the $\sigma_{C\,\min}$ is approximated to σ_{44}, in the Lazar prescription, gives us a hardness of 0.7 GPa. If the Gao model is parameterized with the data obtained with SIESTA, the hardness is 8.1 GPa. Fitting the Zhou model with the published SnO_2 Raman spectrum[59,63] the resulting H_V is 16 GPa.

4. Conclusions

We have found that the elastic properties obtained from *ab initio* calculations combined with DEM can be used for predicting micro Vickers hardness in oxide materials with a wide range of hardness. Their values for rutile TiO_2 is 8.6 GPa in the fail model and 12.28 GPa in the fracture model. These compare well with available experimental $H_V = 11$ GPa obtained at 25 °C. In this phase,the results provided by the models of Chen, Gao, Zhou, are in general agreement with our assessments. In the case of TiO_2 in cotunnite phase, the predicted micro Vickers hardness are 24.08 and 24.41 GPa for the fail and fracture modes respectively, which are in agreement (26 GPa) with very recently theoretical *ab initio* assessment using the Simunek model. Other estimations using Chen, Gao, and Lazar models provide even lower hardness values for the cotunnite phase.

For SnO_2 in the normal rutile phase, the hardness is, in the failure mode, 2.67 GPa, lower than experimental value of *3.68 GPa*. For this phase the Chen, Gao and Zhou models provide even higher value H_V, greater than 8 GPa.

All this evidence, suggest the needs of new experimental research applied to these oxide phases. Especially since experimental microhardness data of TiO_2 and SnO_2 in single crystals, show the importance of critical load of the plastic flow initiation (W). It is noted that this magnitude is significant when compared with the indentation test loads applied.

This work uses a scheme of continuous elasticity theory that employs empirical parameters which is applied in the field of the mechanics of failure and fracture. In our case, we show that the method is able to predict the hardness, if parameterized with converged values obtained from *ab initio* quantum-mechanical calculations.

Then our methodology to obtain the microhardness could be applied to a systematic study of tailoring material. Since hardness is often related to shear elastic properties, our results can be used as a first order assessment of the solid material lubricating properties.

Appendix A. Supplementary data

Supplementary data associated with this article can be found, in the online version, at http://dx.doi.org/10.1016/j.jeurceramsoc.2014.06.022.

References

1. Hebbache M. Shear modulus and hardness of crystals: density functional calculations. *Solid State Commun* 2000;**113**:427–32.
2. Gao F. Theoretical model of intrinsic hardness. *Phys Rev B* 2006;**73**:132104.
3. Gao FM, Gao LH. Microscopic models of hardness. *J Superhard Mater* 2010;**32**:148–66.
4. Dubrovinsky LS, Dubrovinskaia NA. The hardest known oxide. *Nature* 2001;**410**:654.
5. Oganov AR, Lyakhov O. Towards the theory of hardness of materials. *J Superhard Mater* 2010;**32**:143–7.
6. Lyakhov AO, Oganov AR. Evolutionary search for superhard materials applied to forms of carbon and TiO_2. *Phys Rev B* 2011;**84**:092103.
7. Gao F, He J, Wu E, Liu S, Yu D, Zhang S, Tian Y. Hardness of covalent crystals. *Phys Rev Lett* 2003:15502-1–4.
8. Teter DM. Computational alchemy: the search for new superhard materials. *MRS Bull* 1998;**23**:22.
9. Chen X, Niu H, Li D, Li Y. Modeling hardness of polycrystalline materials and bulk metallic glasses. *Intermetallics* 2011;**19**:1275–81.
10. Simunek A, Vackar J. Hardness of covalent and ionic crystals: first principle calculation. *Phys Rev Lett* 2006;**96**:85501.
11. Zhou X, Qian Q, Sun J, Tian Y, Wang H. *Raman model predicting hardness of covalent crystals*. Cornell University Database; 2009 arXiv:0912.4942.
12. Pharr GM, Herbert EG, Gao Y. The indentation size effect: a critical examination of experimental observations and mechanistic interpretations. *Annu Rev Mater Res* 2010;**40**:271.
13. Meyer E. Untersuchungen uber Harteprufung und Harte. *Phys Z* 1908;**9**:66.
14. Hays C, Kendall EG. Analysis of Knoop microhardness. *Metallography* 1973;**6**:275–82.

15. Li H, Bradt RC. The microhardness indentation load/size effect in rutile and cassiterite single crystals. *J Mater Sci* 1993;**28**:917–26.
16. Leger JM, Haines J, Schmidt M, Petitet M, Pereira JP, Da Jornada AS. Discovery of hardest known oxide. *Nature* 1996;**383**:40.
17. He DW, Zhao YS, Daemen L, Shen TD, Zerda TW. Boron suboxide: as hard as cubic boron nitride. *Appl Phys Lett* 2002;**81**:643–5.
18. Caravaca MA, Miño JC, Pérez VJ, Casali RA, Ponce CA. Ab initio study of the elastic properties of single and polycrystal TiO_2, ZrO_2 and HfO_2 in the cotunnite structure. *J Phys Condens Matter* 2009;**21**:015501.
19. Tse JS. Intrinsic hardness of crystalline solids. *J Superhard Mater* 2010;**32**:177–91. ISSN 1063_4576 © Allerton Press, Inc., 2010. Original Russian Text © J.S. Tse, (2010), published in Sverkhtverdye Materialy, 32, (2010), 46–65.
20. Göpel W. Sensors: a comprehensive survey. In: Göpel W, Jones TA, Kleitz M, Lundström I, Seiyama T, editors. *Chemical and Biochemical Sensors I, II*, vols. 2–3. Germany: VCH, Weinheim; 1992.
21. Ihokura K, Watson J. *The stannic oxide gas sensor—principles and applications*. Boca Raton, FL: CRC Press; 1994.
22. Göpel W, Schierbaum KD. SnO_2 sensors: current status and future prospects. *Sens Actuators B* 1995;**26–27**:1–12.
23. Brousse T, Schleich DM. Sprayed and thermally evaporated SnO_2 thin films for ethanol sensors. *Sens Actuators B* 1996;**31**:77–9.
24. Kanazawa E, Kugishima M, Shimanoe K, Kanmura Y, Teraoka Y, Miura N, Yamazoe N. Mixed potential type N_2O sensor using stabilized zirconia- and SnO_2-based sensing electrode. *Sens Actuators B* 2001;**75**:121–4.
25. Allendorf MD. On-line deposition of oxides on flat glass. *Electrochem Soc Interface* 2001;**10**:34–8.
26. Haines J, Léger JM. X-ray diffraction study of the phase transitions and structural evolution of tin dioxide at high pressure: Relationships between structure types and implications for other rutile-type dioxides. *Phys Rev B* 1997;**55**:11144.
27. Hemley RJ. Pressure dependence of Raman spectra of SiO2 polymorphs: α-quartz, coesite, and stishovite. In: Manghnani MH, Syono Y, editors. *High-Pressure Research in Mineral Physics*. Washington, DC: Terra Scientific, Tokyo/American Geophysical Union; 1987. p. 347–59.
28. Niezgoda T, Malachowski J, Boniecki M. Finite elements simulations of Vickers micro-indentation on alumina ceramics. *Ceram Int* 1998;**24**:359–64.
29. Soler JM, Artacho E, Gale JD, García A, Junquera J, Ordejón P, Sánchez-Portal D. The SIESTA method for ab-initio order-N materials simulation. *J Phys Condens Matter* 2002;**14**:2745.
30. Caravaca MA, Casali RA. Ab initio localized basis set study of structural parameters and elastic properties of HfO_2 polymorphs. *J Phys Condens Matter* 2005;**17**:5795.
31. Casali RA, Lasave J, Caravaca MA, Koval S, Ponce CA, Migoni RL. Ab initio and shell model studies of structural, thermoelastic and vibrational properties of SnO_2 under pressure. *J Phys Condens Matter* 2013;**25**:135404.
32. Ouni B, Boukhachem A, Dabbous S, Amlouk A, Boubaker K, Amlouk M. Some transparent semi-conductor metal oxides: comparative investigations in terms of Wemple–DiDomenico parameters, mechanical performance and Amlouk–Boubaker opto-thermal expansivity. *Mater Sci Semiconductor Process* 2010;**13**(4):281–7.
33. DellaCorte C, Deadmore DL. *Vickers Indentation_Hardness of Stoichiometric and Reduced Single Crystal TiO_2 (Rutile) from 25 to 800 °C*. NASA Technical Memorandum 105959, April; 1993.
34. Cundall PA, Strack ODL. A discrete numerical model for granular assemblies. *Geotechnique* 1979;**29**:47.
35. Riera JD. Local effects in impact problems on concrete structures. In: *Proceedings, Conference on Structural Analysis and Design of Nuclear Power Plants*. 1984 [CDU 264.04:621.311.2:621.039].
36. Nayfeh AH, Hefzy MS. Continuum modeling of three dimensional trusslikespace structures. *AIAA J* 1978;**16**:779–87.
37. Hillerborg A. *A model for fracture analysis*; 1971. Cod. LUTVDG/TVBM 300-51-8.
38. Kosteski LE, Barrios R, Iturrioz I. Crack propagation in elastic solids using the truss-like discrete element method. *Int J Fract* 2012, doi:10.1007/s10704-012-9684-4.
39. Kosteski LE, Iturrioz I, Batista RG, Cisilino AP. The truss-like discrete element method in fracture and damage mechanics. *Eng Comput* 2011;**6**:765–87.
40. Tromans D, Meech JA. Fracture toughness and surface energies of minerals: theoretical estimates for oxides, sulphides, silicates and halides. *Miner Eng* 2002;**15**:1027–41.
41. Zhao J, Wang G, Liang Y. Mechanical properties and electronic structures of cotunnite TiO_2. *Chin Phys Lett* 2008;**25**:4356.
42. Shojaee E, Abbasnejad M, Saeedian M, Mohammadizadeh MR. First-principles study of lattice dynamics of TiO_2 in brookite and cotunnite structures. *Phys Rev B* 2011;**83**:174302.
43. Chang E, Graham EK. The elastic constants of cassiterite SnO_2 and their pressure and temperature dependence. *J Geophys Res* 1975;**80**(17):2595–9.
44. Wachtman Jr JB, Tefft WE, Lam Jr DG. Elastic constants of rutile (TiO2). *J Res Natl Bur Stand: Phys Chem* 1962;**66A**:465–71.
45. Isaak DG, Carnes JD, Anderson OI, Cynn H, Hake E. Elasticity of TiO_2 rutile to 1800 K. *Phys Chem Miner* 1998;**26**:31.
46. Vick GL, Hollander LE. Ultrasonic measurement of the elastic moduli of rutile. *J Acoust Soc Am* 1960;**32**:947.
47. Zhu B, Liu Ci, Lv M, Chen X, Zhu J, Ji G. Structures, phase transition, elastic properties of SnO_2 from first-principles analysis. *Physica B* 2011;**406**:3508–13.
48. Liu Chun-Mei, Chen Xiang-Rong, Ji Guang-Fu. First-principles investigations on structural, elastic and electronic properties of SnO_2 under pressure. *Comput Mater Sci* 2011;**50**:1571–7.
49. Wang Y, Chang J, Tan L, Chen X. Elastic properties of rutile TiO_2 at high temperature. *Chin Phys Lett* 2007;**24**:2642.
50. Kim HC, Park HK, Shon In, Ko IY. Fabrication of ultra-fine TiO_2 by a high-frequency induction heating sintering method. *J Ceram Process Res* 2006;**7**:327–31.
51. http://www.ndt.net/article/SimNDT2010/papers/12_Caravaca.pdf
52. $C_{11} = \frac{2 \cdot E_A}{Lc^2} \cdot \left(1 + \frac{4}{9} \cdot \delta\right) \quad C_{12} = \frac{E_A \cdot v}{(1+v) \cdot (1-2v)}$.
53. O'Neill H. *The hardness of metals and its measurement*. Cleveland, OH: Sherwood; 1934. p. 43.
54. Mott BW. *Micro-indentation hardness testing*. London: Butterworths Scientific; 1956. p. 101.
55. Gane N, Cox JM. The micro-hardness of metals at very low loads. *Philos Mag* 1970;**22**:881–91.
56. $\frac{\langle H_V \exp \rangle}{H_V} = \frac{\langle F \rangle}{\langle F \rangle - \langle W \rangle}; \quad H_V = 0.8 \langle H_V \exp \rangle$.
57. Ding Y, Chen M, Wu W. Mechanical properties hardness and electronic structure of new post cotunnite phase (Fe2P-type) of TiO_2. *Phys B* 2014;**433**:48–54.
58. Lazar P, Chen X, Podloucky R. First-principles modelling of hardness in transition–metal diborides. *Phys Rev B* 2009;**80**:012103.
59. Sun SH, Meng GW, Zhang GX, Gao T, Geng BY, Zhang LD, Zuo J. Raman scattering study of rutile SnO_2 nanobelts synthesized by thermal evaporation of Sn powders. *Chem Phys Lett* 2003;**376**:103–7.
60. Al-Khatatbeh Y, Lee KKM, Kiefer B. High-pressure behavior of TiO_2 as determined by experiment and theory. *Phys Rev B* 2009;**79**:134114.
61. Nishio-Hamane D, Shimizu A, Nakahira R, Niwa K, Furukawa AS, Okada T, Yagi T, Kikegawa T. The stability and equation of state for the cotunnite phase of TiO_2 up to 70 GPa. *Phys Chem Miner* 2010;**37**:129–36.
62. Nicol N, Fong MY. Raman spectrum and polymorphism of titanium dioxide at hight pressure. *J Chem Phys* 1971;**54**:3167–70.
63. Lupan O, Chow L, Chai G, Schulte A, Park S, Heinrich H. A rapid hydrothermal synthesis of SnO_2 nanowires. *Mater Sci Eng B* 2009;**157**:101–4.